C h a p t e r 3

TUNABLE THERMAL BIOSWITCHES FOR IN VIVO CONTROL OF MICROBIAL THERAPEUTICS

Piraner, D. I., Abedi, M. H., Moser, B. A., Lee-Gosselin, A., & Shapiro, M. G. (2017). Tunable thermal bioswitches for in vivo control of microbial therapeutics. *Nature Chemical Biology*, *13*(1), 75–80. https://doi.org/10.1038/nchembio.2233

3.1: Introduction

Rapid advances in synthetic biology[1, 2] are driving the development of genetically engineered microbes as therapeutic[3-6] and diagnostic[7-10] agents for a multitude of human diseases. A critical capability for many envisioned applications is the ability to control the function of engineered microbes *in situ* to enable spatially and temporally specific activation at anatomical and disease sites such as the gastrointestinal tract or tumors[2]. However, among existing control methods, systemic chemical administration typically lacks the spatial precision needed to modulate activity at specific anatomical locations, while optical approaches suffer from poor light penetration into tissues[11]. On the other hand, temperature can be controlled both globally and locally – at depth – using technologies such as focused ultrasound[12], infrared light[13] and magnetic particle hyperthermia[14]. In addition, body temperature can serve as an indicator of microbial entry and exit from the host organism and of the host's condition (*e.g.*, fever).

Given this potential, remarkably few high-performance thermal bioswitches are available to control gene expression in engineered microbes. The ideal bioswitch should have a sharp thermal transition resulting in a large change in activity (> 100-fold over a few degrees), and its switching temperature should be tunable to enable a broad range of applications. In addition, the bioswitch should be orthogonal to endogenous cellular machinery and compatible with other thermo-responsive components to allow multiplexed thermal logic. Existing temperature-dependent regulators of gene expression – including microbial heat shock factors, membrane-associated proteins, RNA thermometers, and transcriptional repressors – fail to fulfill these criteria. Microbial heat shock promoters undergo a relatively low level of thermal induction (~10-fold)[15], have crosstalk with other stimuli such as chemical stress[16], and may be difficult to tune without deleterious effects on the cell. Likewise, the switching temperature of membrane-associated proteins depends on bilayer composition and occupies second messenger pathways[17]. Meanwhile, RNA thermometers, while orthogonal to the host and amenable to tuning, generally have small dynamic ranges (< 10-fold) and broad transitions (> 10 °C)[18-25]. Of the available molecular machinery, several natural and mutant transcriptional repressors have the most robust thermal switching and potential for orthogonality[26-32]. However, their relative performance has not been characterized, they have not been systematically engineered to operate at specific transition temperatures, and their potential utility for *in vivo* microbial therapy applications has not been demonstrated.

To address the need for robust, tunable, orthogonal thermal control of engineered microbial systems, we systematically screened candidate transcriptional regulators, developed two

orthogonal families of high-performance thermal bioswitches with tunable thresholds within the biomedically relevant range of 32ºC to 46ºC, and demonstrated the potential utility of these devices in three distinct *in vivo* scenarios relevant to mammalian microbial therapy. These scenarios include spatially selective activation within a mammalian host using focused ultrasound, sensing and response to a fever, and self-destruction at ambient temperatures to prevent environmental contamination after leaving the intended host.

3.2: Results

3.2a: High-Performance Thermal Bioswitches

In order to engineer new families of robust, tunable, orthogonal thermal bioswitches, we began by characterizing the performance of six temperature-dependent transcriptional repressors and six endogenous heat shock promoters. Our panel included TlpA, a transcriptional autorepressor from the virulence plasmid of *Salmonella typhimurium*. This protein contains an approximately 300 residue C-terminal coiled-coil domain that undergoes sharp, temperature-dependent uncoiling between 37ºC and 45ºC , and an N-terminal DNA binding domain that, in its low-temperature dimeric state, blocks transcription from the 52 bp TlpA operator/promoter[26, 32]. In addition, we tested a well-known temperature-sensitive variant of the bacteriophage λ repressor cI (mutant cI^{857}, here referred to as TcI) acting on a tandem pR/pL operator/promoter[27]. In most previous applications, TcI repression has been modulated via large changes in temperature (e.g., steps from 30°C to 42°C)[27]. However, its original description as a virulence factor suggested that much sharper switching may be

possible[28]. Alongside TlpA and TcI, we tested four reported temperature-sensitive mutants of the *E. coli* repressors TetR (A89D and I193N)[29] and LacI (A241T and G265D)[30, 31], together with a panel of endogenous heat shock promoters, including GrpE, HtpG, Lon, RpoH, Clp and DnaK (**Fig. 3-1a**).

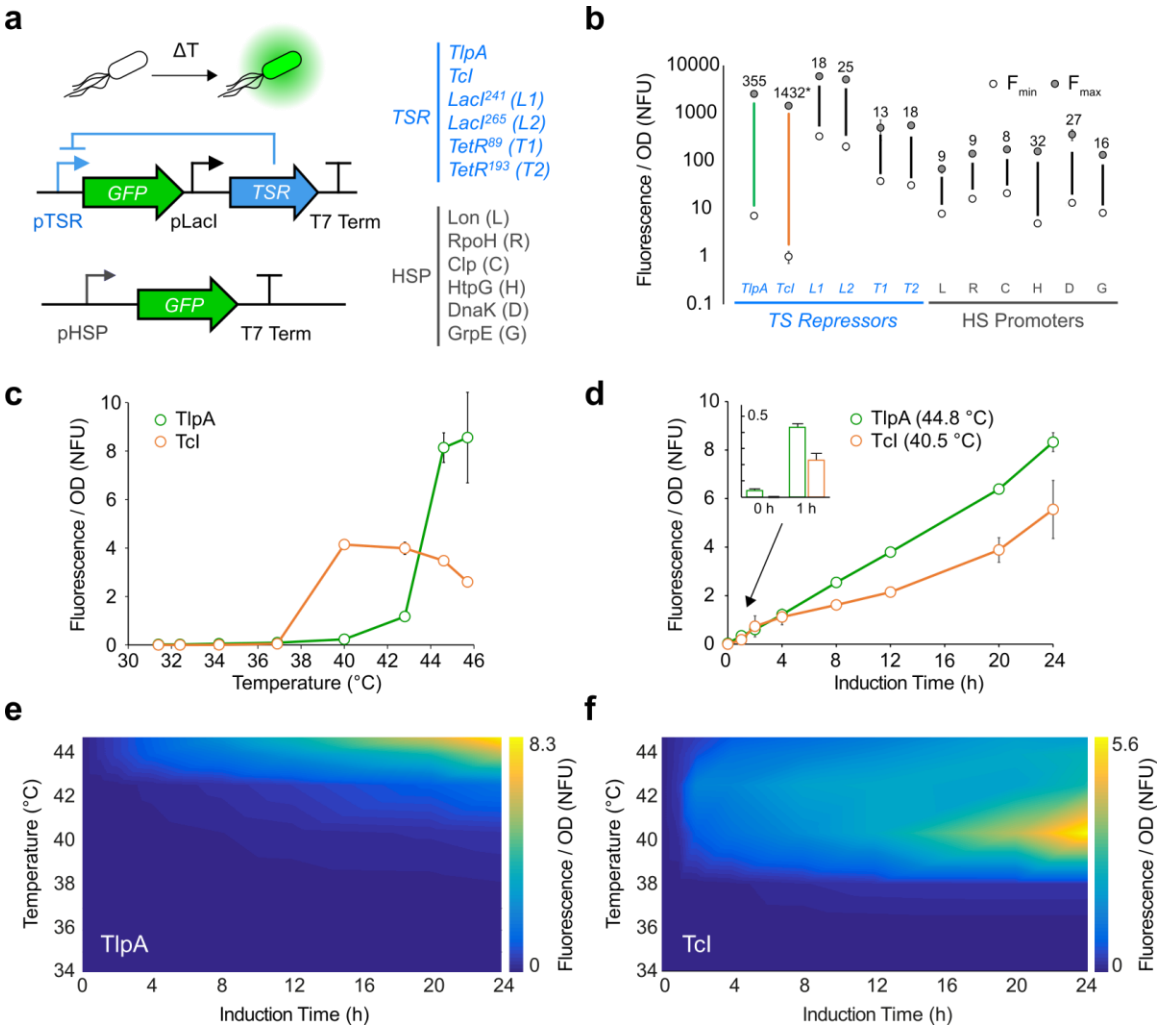

Figure 3-1: High-performance thermal bioswitches. (**a**) Constructs used to assay the performance of temperature-sensitive repressors (TSr, top) and heat shock promoters (HSP, bottom). The specific repressors and promoters assayed are listed in blue and gray, respectively. (**b**) optical density (oD)-normalized fluorescence after 12 h of thermal induction for the constructs shown in a. nFu, normalized fluorescence units. Fmin represents expression at 31.4 °C; Fmax is the maximum fluorescence intensity measured for each construct, measured up to 45.7 °C. The fold changes between Fmin and Fmax are listed above each sample. Where not seen, error bars are smaller than the symbol. N = 4 for TSrs and N = 3 for HSPs. The Fmin for TcI (indicated by *) is reported from

measurement at 34.2 °C because expression at lower temperatures was below the detection limit of the assay. (**c**) oD-normalized fluorescence from the Tlpa- and TcI-regulated constructs as a function of induction temperature for a fixed duration of 12 h. N = 4. (**d**) oD-normalized fluorescence as a function of thermal induction duration at the maximal induction temperature for the Tlpa and TcI constructs. N = 4. (**e**,**f**) oD-normalized fluorescence landscapes for Tlpa- and TcI-gated constructs, respectively, as a function of both incubation temperature and duration. Data shown interpolated from an 8 × 8 sampling matrix. all samples in d–f were maintained at 30 °C after the indicated period of thermal induction for a total experimental duration of 24 h before measurement. Error bars represent ± s.e.m.

The performance of these constructs is summarized in **Figure 3-1b**. TlpA and TcI had by far the largest dynamic ranges (355 ± 45 and >1,432, respectively), reflecting a combination of tighter repression at sub-threshold temperatures and stronger promoter activity above threshold. Both of these repressors show sharp thermal transitions, with greater than 30-fold induction over ranges of 5ºC and 3ºC centered at 43.5°C and 39.5ºC for TlpA and TcI, respectively (**Fig. 3-1c**). Furthermore, both systems are capable of rapid induction, with greater than 10-fold changes in expression observed after a 1 hour thermal stimulus (**Fig. 3-1d**). Complete time-temperature induction profiles for TlpA and TcI are shown in **Figure 3-1, e–f**. In addition to their high performance, TlpA and TcI are expected to be more orthogonal to cellular machinery than both the native heat shock promoters and the engineered TetR and LacI repressors, the latter of which are utilized in multiple endogenous and engineered gene circuits[33-35]. A homology search[36] showed that TlpA and TcI repressors are present in far fewer bacterial species than either TetR or LacI (**Supplementary Fig. 3-S1**). Based on these factors, we chose TlpA and TcI as our starting points for further bioswitch engineering.

Since the TlpA operator/promoter has not been studied in *E. coli*, we characterized its molecular mechanisms to inform its utilization in genetic circuits. As shown in

Supplementary Figure 3-S2, the TlpA operator is a strong promoter (88-fold stronger than $LacI^Q$) driven by the transcription factor σ^{70}. Interestingly, this promoter has bidirectional activity with identical thermal regulation in both orientations, but approximately 200-fold lower maximal expression in the reverse direction (**Supplementary Fig. 3-S2, c–d**). This property will enable convenient adjustment of TlpA-regulated expression according to circuit requirements.

3.2b: Tuning Bioswitch Activation Temperatures

Applications in microbial therapy require thermal bioswitches that activate at different transition temperatures. For example, a host colonization sensor should be activated at 37ºC, while a fever detector may work best with a thermal threshold of 39ºC, and a focused ultrasound-activated switch may require a transition point of 41ºC to avoid nonspecific actuation. Synthetic biology applications outside biomedicine may likewise have a variety of thermal requirements. It is thus highly desirable to be able to tune thermal bioswitches to activate at new temperatures while retaining sharp, robust switching performance. To enable such tuning of TlpA and TcI, we devised a simple and effective high-throughput assay based on colony fluorescence. We grew *E. coli* expressing GFP under the control of mutant repressors (generated by error-prone PCR) on solid media and replica-plated the colonies onto separate plates for simultaneous incubation at desired "off" and "on" temperatures (**Supplementary Fig. 3-S3a**). We then imaged the plates with wide-field fluorescence, as shown in **Figure 3-2a**. As expected, many colonies show constitutive expression (ostensibly due to loss of repressor function) while others fail to de-repress (most likely retaining their

original high transition point). However, several colonies show thermal induction in the desired regime. Within each screen, we selected several such colonies to undergo liquid phase characterization of induction temperature, switching sharpness, and expression levels (**Fig. 3-2b**). From these variants, we selected mutants that retained the desirable performance characteristics of the wild type repressor, but with shifted transition temperatures.

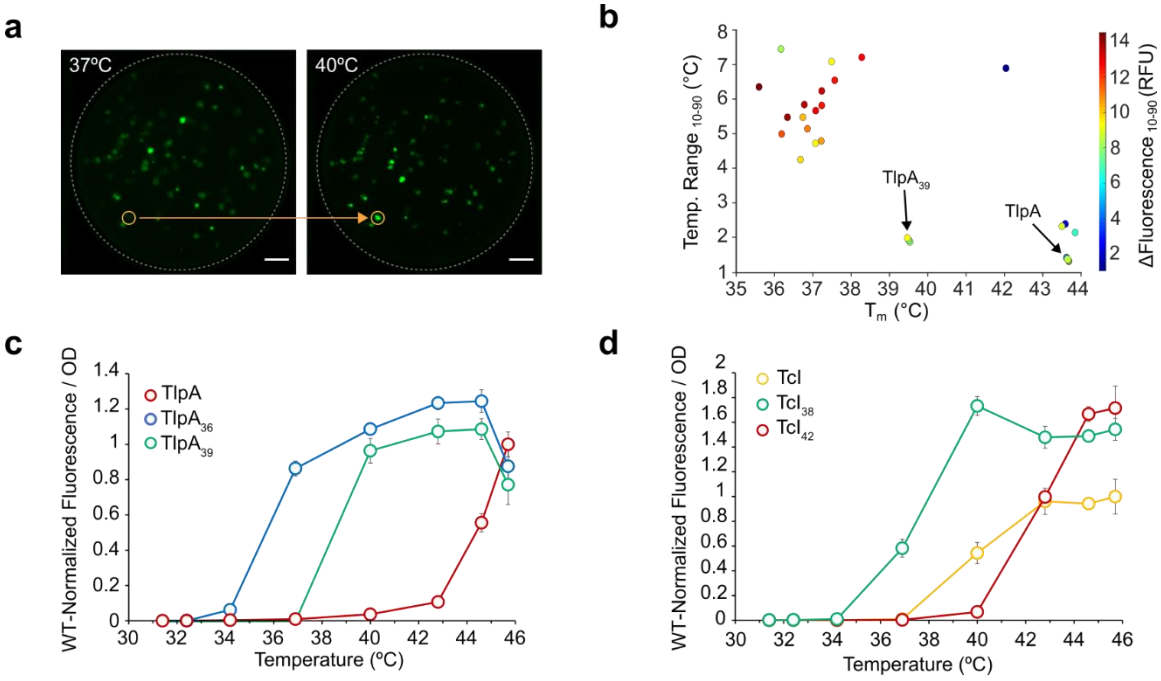

Figure 3-2: Tuning the transition temperature of thermal bioswitches. (**a**) Fluorescence image of replica plates used to screen for TlpA variants turning on between 37 °C and 40 °C. One colony selected for further assay is indicated by the orange circle. Scale bars, 1 cm. (**b**) TlpA variants plotted by their measured midpoint transition temperatures (T50) and 10–90% transition range (T10–90), estimated by linear interpolation. The color of each data point maps to the change in fluorescence over the T10–90 span. (**c**) OD-normalized fluorescence of the novel Tlpa variants normalized to wild type (WT). (**d**) OD-normalized fluorescence of the novel TcI variants normalized to wild type. N = 4 for c and d. RFR, relative fluorescence units. Error bars represent ± s.e.m.

Screening of TlpA mutants at off-on temperatures of 30–37ºC and 37–40ºC produced high-performance bioswitches centered at 36 °C and 39 °C, respectively, which we named $TlpA_{36}$ and $TlpA_{39}$ (**Fig. 3-2c**). For TcI, we selected both downshifted (TcI_{38}, T_m = 38 °C) and upshifted (TcI_{42}, T_m = 42 °C) variants relative to the original protein (**Fig. 3-2d**). Together,

the engineered TlpA and TcI repressor families cover the biomedically relevant range of 32ºC to 46ºC (**Supplementary Fig. 3-S3b**) while demonstrating a dynamic range similar to that of the wild type protein (**Supplementary Table 3-T1**). The amino acid substitutions identified in these bioswitch variants are shown in **Supplementary Figure 3-S4**. The observed decrease in fluorescence at the highest temperatures tested may be due to thermal instability of the cell's transcriptional and translational machinery. Remarkably, a single round of mutagenesis was sufficient in all cases to obtain at least one variant with the desired switching behavior, suggesting that both TlpA and TcI are highly tunable for a broad range of applications.

3.2c: Thermal Logic Circuits Using Orthogonal Bioswitches

To enable microbial therapy applications, it is useful to develop thermal logic circuits capable of controlling multiple functions at different temperatures or confining activity to within a narrow thermal range. This would enable cells to, for example, initiate one therapeutic function upon host colonization and switch to a different function during a host fever response or local activation with focused ultrasound. We hypothesized that since TlpA and TcI act on orthogonal target sequences, we could combine them in circuits designed for multiplexed thermal control or band-pass activation of microbial function. To assess the first possibility (**Fig. 3-3a**), we made a construct encoding a GFP modulated by $TlpA_{36}$ and an RFP regulated by TcI (**Fig. 3-3b**). As predicted, upon exposure to a range of temperatures, the two reporter genes were activated independently at their expected thresholds, with no apparent crosstalk in their induction (**Fig. 3-3c**). Independent thermal control of the co-

expressed circuits is illustrated by spatially patterned bacterial variants incubated at 37ºC and 42ºC (**Fig. 3-3d**). Next, to develop a thermal band-pass filter (**Fig. 3-3e**), we engineered a circuit placing the expression of RFP under the control of the lambda operator, gated by both TcI (turning on above 36ºC) and the temperature-independent wild type cI repressor, which was itself placed under the control of TlpA (activating above 43ºC) as shown in **Figure 3-3f**. The cI open reading frame was preceded by a T7 terminator and a weak ribosome binding site to reduce buildup of this repressor at 40–43 °C due to leakage of the upstream TlpA operon. This resulted in RFP expression confined between 36 and 44ºC, while simultaneously turning on GFP above RFP's turn-off temperature (**Fig. 3-3, g–h**).

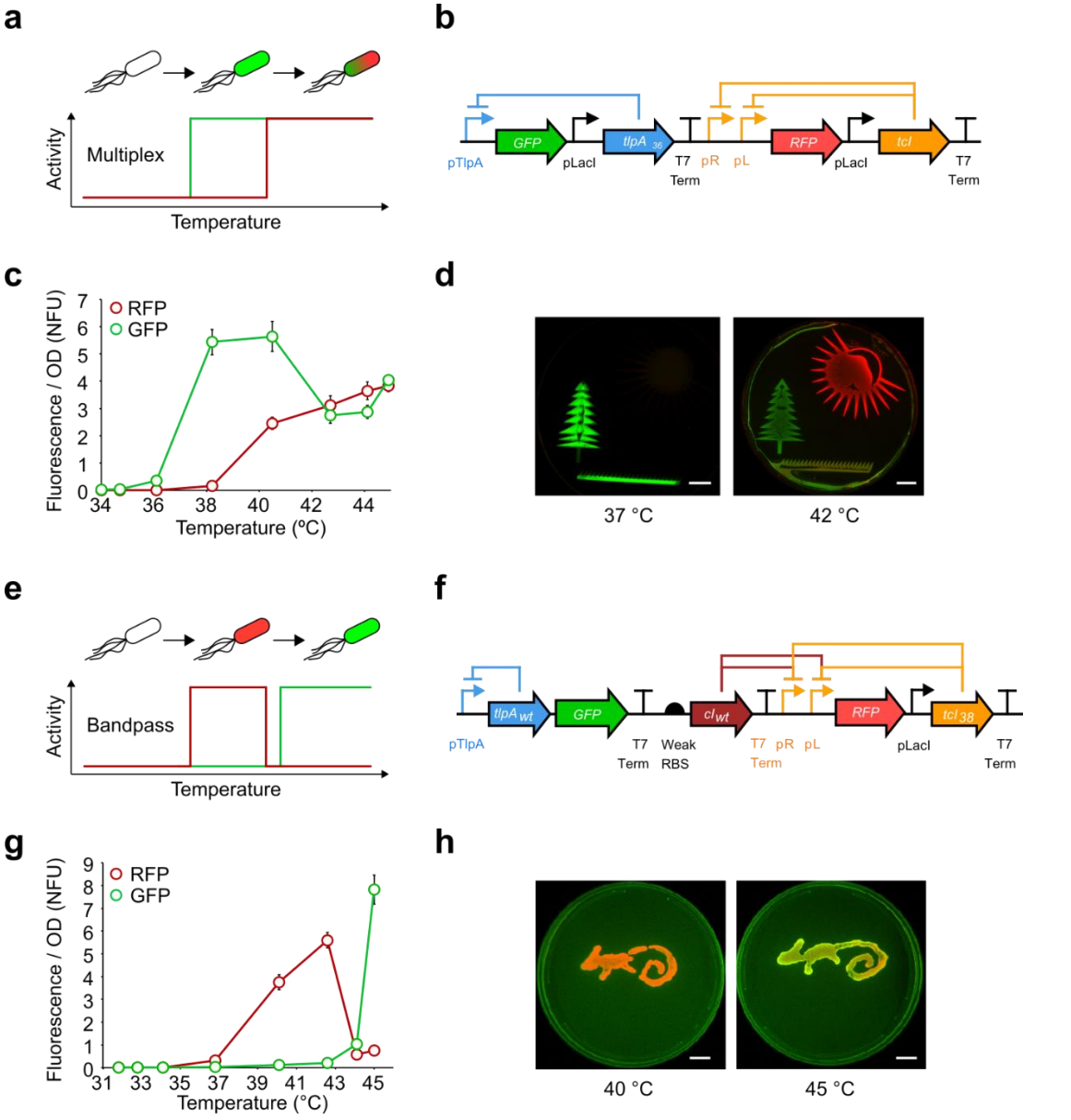

Figure 3-3: Thermal logic circuits. (**a**) Diagram illustrating multiplexed thermal activation. (**b**) Circuit diagram of the pCali2 plasmid, which contains GFP gated by $TlpA_{36}$ and RFP gated by TcI. (**c**) Expression of GFP and RFP from pCali2-containing *E. coli* over the indicated range of temperatures (12-h incubation). (**d**) Plate images of overlaid GFP and RFP fluorescence from the pCali2 plasmid (grass) and plasmids expressing only the green (tree) and red (sun) components. Note that at 42 °C the grass shows both green and red fluorescence. (**e**) Diagram illustrating a thermal bandpass filter. (**f**) Circuit diagram of the pThermeleon plasmid, in which RFP is gated by TcI_{38} and also by the wild-type cI repressor. GFP is gated by $TlpA_{wt}$ on the same plasmid, which also weakly drives the expression of cI_{wt} through a T7 terminator and weak ribosome-binding site. (**g**) Thermal expression profile of RFP and GFP from pThermeleon-containing *E. coli* (12 h incubation). (**h**) Overlaid GFP and RFP fluorescence images of plated bacteria containing pThermeleon cultured at 40 °C and 45 °C. Scale bars, 1 cm. N = 4 for **c** and **g**. Error bars represent ± s.e.m.

3.2d: Spatially Targeted Control Using Focused Ultrasound

After developing TlpA and TcI-based thermal bioswitches, we demonstrated their utility in three prototypical microbial therapy scenarios. First, we tested the ability of thermal bioswitches to mediate spatially-selective control of microbial therapies using focused ultrasound, a modality that is well established in its ability to elevate temperatures in deep tissues with millimeter spatial precision [12] and utilized clinically to treat diseases such as cancer[37] and essential tremor[38]. Focused ultrasound has been used to activate gene expression in mammalian cells[39], but has not, to our knowledge, been employed to control the activity of microbes *in vivo*. Such control could be highly advantageous in applications where the activity of a systemically administered microbial therapy needs to be localized to a specific anatomical site, such as a deep-seated tumor or section of the gastrointestinal tract, which would be difficult to reach with optogenetic triggers. To test this concept, we first activated gene expression using focused ultrasound in tissue-mimicking phantoms under the guidance of magnetic resonance imaging (MRI)[40] (**Fig. 3-4a**). This guidance enabled precise spatial targeting of the ultrasound focus and real-time monitoring and adjustment of local temperature. We first applied this technique to a flat lawn of *E. coli* containing the multiplexed expression circuit shown in **Figure 3-3b**. This specimen was assembled with a tissue-mimicking tofu phantom, and steady-state focal heating over 45 minutes resulted in a radial thermal gradient with an average focal temperature of 42ºC, as observed by real-time MRI thermometry (**Fig. 3-4b**). A corresponding pattern of spatially localized fluorescence is seen in **Figure 3-4c**.

To establish the feasibility of this approach *in vivo*, we injected *E. coli* expressing GFP under the control of $TlpA_{36}$ subcutaneously into both hindlimbs of a nude mouse and applied MRI-guided focused ultrasound to one location (**Fig. 3-4d**) to produce a local steady-state temperature of 41ºC for 45 min to 1 hour. This thermal dose is below the damage thresholds for mammalian tissues such as muscle and brain[41, 42]. *In vivo* fluorescence imaging four hours after ultrasound treatment showed robust expression of GFP specifically at the ultrasound-targeted anatomical site (**Fig. 3-4e**). Two additional animals undergoing the same procedure are shown in **Supplementary Figure 3-S5**. $TlpA_{36}$ was selected as the thermal bioswitch for these experiments because its activation threshold is approximately 4ºC above the typical murine cutaneous temperature[43], a sufficient difference for site-specific ultrasound activation.

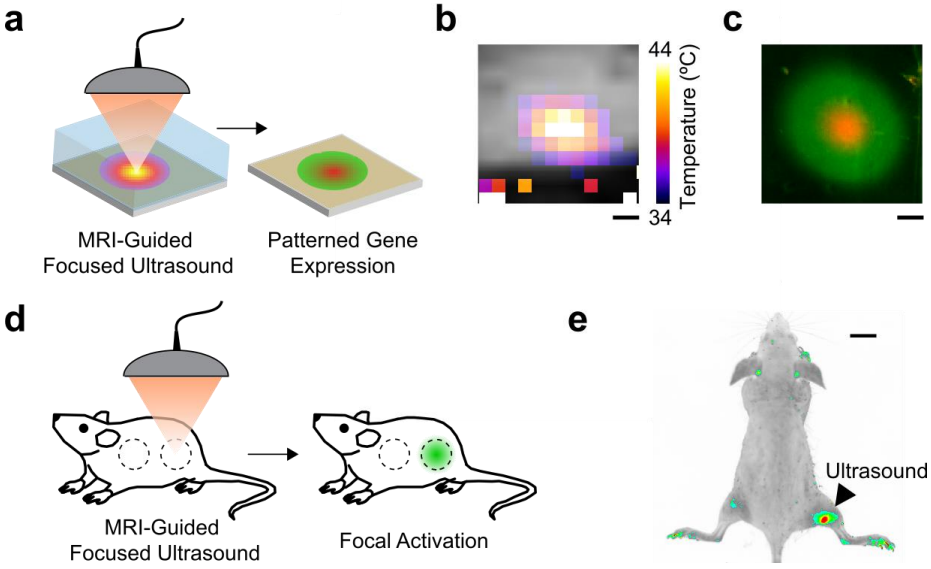

Figure 3-4: Remote control of bacterial agents using focused ultrasound. (**a**) Illustration of the *in vitro* focused ultrasound experiment: focused ultrasound is used to heat a target area of a bacterial culture lawn through a tofu phantom (depicted as translucent) under MRI guidance, followed by fluorescence imaging. (**b**) MRI-based temperature map of the bacterial specimen during steady-state ultrasound application, overlaid on a raw grayscale MRI image of the phantom. (**c**) Fluorescence image of the region targeted by ultrasound, showing activation consistent with a bacterial construct expressing GFP under the control of $TlpA_{36}$ and RFP regulated by TcI. (**d**) Illustration of the *in vivo* experiment, in which focused ultrasound is used to activate subcutaneously injected bacterial agents

at a specific anatomical site. (**e**) Representative thresholded fluorescence map of a mouse injected subcutaneously in both left and right hindlimbs with *E. coli* expressing GFP under the control of $TlpA_{36}$, following ultrasound activation directed at only the right hindlimb. Scale bars, 2 mm (**b**,**c**) and 1 cm (**e**).

3.2e: Programmed Responses to Mammalian Host Temperature

Next, we sought to develop autonomous thermosensitive microbes responsive to endogenous changes in host temperature. First, we investigated whether bacteria can be engineered to sense and respond to a host fever (**Fig. 5a**). We subcutaneously injected one flank of a nude mouse with *E. coli* expressing GFP under the control of $TlpA_{36}$, and the other flank with *E. coli* expressing GFP controlled by wild type TlpA as a high-threshold control for non-specific activation. The mouse was then housed at 41ºC for two hours in an established fever model paradigm[44]. *In vivo* fluorescent imaging four hours after fever induction shows robust expression of GFP in the flank injected with $TlpA_{36}$–regulated bacteria (**Fig. 5b**). No significant activation is seen in the opposite flank or in a mouse housed at room temperature (**Fig. 5c**). Two additional replicates of this experiment are shown in **Supplementary Figure 6**.

Second, we tested whether a thermal bioswitch operating at 37ºC could be used to confine the activity of genetically engineered microbes to the *in vivo* environment of a mammalian host and thereby limit the potential for environmental contamination. Towards this end, we designed a genetic circuit in which $TlpA_{36}$ controls the expression of CcdA, a bacterial antitoxin, while constitutively expressing the toxin CcdB, thereby restricting growth to temperatures above 37ºC (**Fig. 5d**). A degradation tag was fused to CcdA to accelerate cell

death at non-permissive temperatures. Bacteria carrying this plasmid grew normally above this permissive temperature, while bacteria incubated at 25ºC had significantly reduced survival as demonstrated by their CFU counts in **Figure 5e**. We administered these bacteria to mice by oral gavage and collected fecal pellets after five hours to allow transit through the gastrointestinal tract. The pellets were kept for 24 hours at either 25ºC, corresponding to excretion into the ambient environment, or at 37ºC, equivalent to persistent residence in the gut, and subsequently assayed for colony formation. The survival of cells excreted into ambient temperature was reduced by ten thousand fold compared to cells maintained under host conditions (**Fig. 5f**).

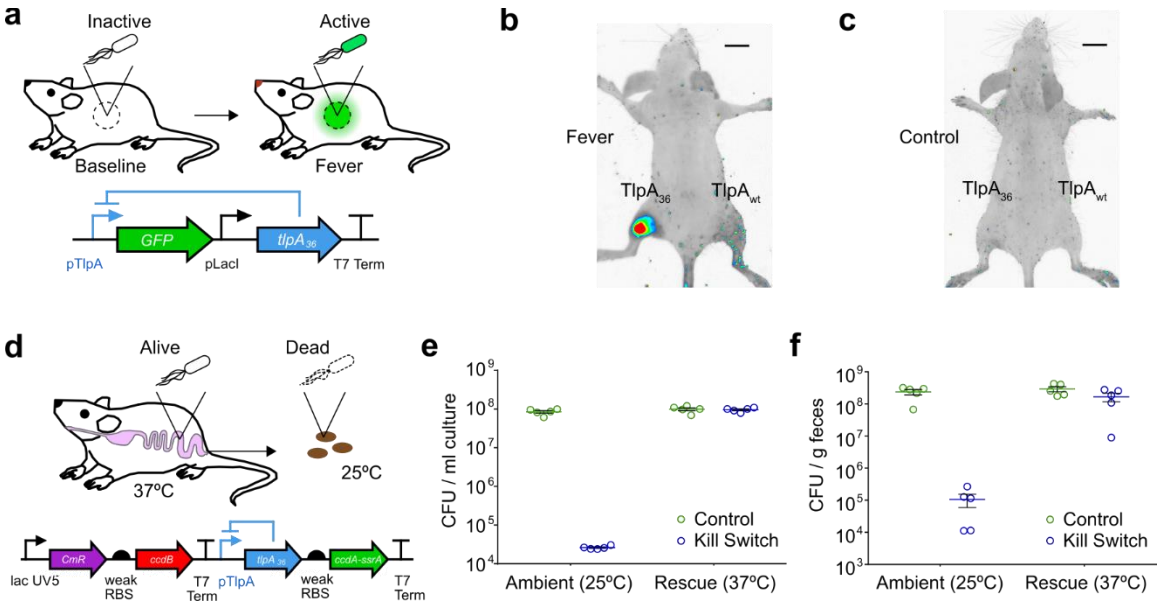

Figure 3-5: Programmed responses to mammalian host temperature. (**a**) Illustration of the fever-induced activation experiment and circuit diagram of the corresponding *E. coli* construct. (**b**) Representative thresholded fluorescence map of a mouse that underwent fever induction after being injected subcutaneously with plasmids expressing TlpaA$_{36}$- and TlpA-regulated GFP into the left and right hindlimbs, respectively. (**c**) Representative thresholded fluorescence map of a mouse that was prepared identically to the animal in **b** but maintained at room temperature. (**d**) Illustration of the temperature- based host confinement strategy, and circuit diagram of the thermal kill switch permitting bacterial survival only at temperatures above 36 °C, at which antitoxin expression is derepressed by TlpA$_{36}$. (**e**) Colony counts from liquid cultures of kill-switch-containing cells and controls (containing no toxin system) after 24 h of incubation at the indicated temperature. P = 0.0002

for kill switch versus control cells at 25 °C and P < 0.0001 for kill switch at 25 °C versus 37 °C. N = 5. (**f**) Colony counts in fecal samples freshly collected from N = 5 mice 5 h after oral gavage of kill-switch-containing *E. coli* or controls. The feces were incubated at a temperature representative of post-defecation conditions (25 °C) or were rescued at 37 °C. P = 0.0067 for kill switch versus control cells at 25 °C and P = 0.0275 for kill switch at 25 °C versus 37 °C. N = 5. Error bars represent ± s.e.m. Scale bars, 1 cm.

3.3: Discussion

Our results establish two new families of high-performance, orthogonal thermal bioswitches with tunable activation thresholds to enable a variety of biotechnology applications. Both TlpA- and TcI-based switches respond to temperature with hundreds-fold changes in gene expression. If needed, this response could be further boosted using well-established strategies such as tandem operators and positive feedback amplification[45, 46]. In addition, the temporal response of thermal bioswitch circuits could be made either more transient, by manipulating the lifetime of the resulting transcripts and proteins, or longer-lasting using genetic toggle switches or recombinase-based architectures[30, 47]. This may enable persistent functions to be controlled with thermal stimuli shorter than those used in this study.

Our strategy for tuning the thermal response of TlpA and TcI is rapid and simple to implement. The fact that we could identify high-performance variants with new transition temperatures by screening several hundred mutants suggests that many different sequences could satisfy a given thermal requirement. Here, we focused on bioswitches operating between 32 and 46ºC, in keeping with potential therapeutic applications and the thermal tolerance of our bacterial chassis. We expect that a similar selection strategy using thermophilic or cryophilic bacteria could be used to tune TlpA and TcI over a yet broader temperature range for industrial applications such as biofuel production. The thermal stability

of the regulated gene product will need to be taken into account in these scenarios. Within the temperature range tested in this study, GFP, RFP and CcdA were functional.

The presented bioswitches have sequences orthogonal to bacterial host machinery and to each other, enabling multiplexed thermal actuation. If desired, additional multiplexing could be accomplished by replacing the DNA-binding domains of TlpA or TcI with those of other dimeric repressors. Additional engineering may be needed to adapt this technology to other host organisms. Certain species of therapeutic microbes, such as *Lactobacillus spp.*, are able to use some promoters transferred directly from *E. coli*[48]. Others may require incorporation of the relevant operator sequences into promoters native to the host[49]. Alternatively, fusions of TlpA and TcI with DNA binding domains from other microbes or eukaryotes could adapt TlpA and TcI for use in these species.

The three *in vivo* scenarios demonstrated in this work will inform the use of thermal bioswitches in future microbial therapy applications. For example, the ability to detect a host's fever provides a potential safety mechanism with which to curtail effector activity in response to runaway inflammation, a major and sometimes lethal side-effect of antitumor cell therapy[50]. In addition, temperature-dependent kill switches can be used to restrict the survival of enterically-administered microbes to host body temperature and thereby mitigate the risk of patients shedding genetically modified, pharmaceutically active organisms into the surrounding environment. Such kill switches can be incorporated into recently developed multilayered and multi-input containment circuits for greater efficiency in preventing mutational escape[51, 52]. Furthermore, the ability to activate microbial function at specific anatomical sites using focused ultrasound opens new therapeutic avenues by potentially

allowing a physician to locally target therapeutic effects that would be intolerable via systemic administration. Additionally, the ability to trigger gene expression *in vivo* can be combined with genetically encoded genomic or proteomic tools[53-55] to enable the study of cellular signaling within the context of mammalian hosts.

3.4: Methods

Plasmid Construction and Molecular Biology

All constructs were made via restriction cloning, KLD mutagenesis, or Gibson Assembly using enzymes from New England Biolabs. All plasmids and their sources of genetic material are described in **Supplementary Table 3-T2**. All constructs were cloned in Mach1 *E. coli* (Thermo Fisher) and the sequence-validated plasmids were assayed in NEB10β *E. coli* (NEB). Fluorescent reporters referred to in the text as GFP and RFP are mWasabi and mCherry, respectively[56, 57].

Thermal Regulation Assay

2 mL cultures of 2xYT media with 100 µg/mL ampicillin were inoculated with a single colony per culture and grown at 30 °C, 250 rpm for 20 hours. After dilution to OD_{600} = 0.1 in LB (Sigma) with 100 µg/mL ampicillin, the cells were propagated at 30 °C, 250 rpm for 1.5 hours, after which OD_{600} was measured using a Nanodrop 2000c (Thermo Scientific) in cuvette mode every 10 minutes. At OD_{600} = 0.25, the cultures were dispensed in 25 µL aliquots into 8 well PCR strips with optically transparent caps (Bio-Rad) using a multichannel pipette and placed into a spatial temperature gradient formed by a Bio-Rad C1000 Touch thermocycler with the lid set to 50 °C. The temperature in each thermocycler

well was verified using a TEF-30-T thermocouple (J-KEM Scientific) immersed in 25 µL of pure water within a PCR tube. After the prescribed thermal stimulus, PCR strips were removed, vortexed, spun down on a tabletop centrifuge and the fluorescence was measured using a Stratagene MX3005p qPCR (Agilent). Immediately after measurement, the cultures were diluted with 75 µL LB/Amp and mixed, after which 90 µL of culture was transferred into 96 well plates (Costar black / clear bottom) for measurement of OD_{600} using a SpectraMax M5 plate reader (Molecular Devices). For studies of gene expression as a function of thermal induction time (Fig. 1, d–f), samples were returned to incubation at 30 °C after their indicated thermal induction periods such that the total experimental duration was 24 hours. Fluorescence measurements were made at the end of this period. Gene expression (*E*) was determined according to Equation 1:

$$E = \frac{F_{sample} - F_{blank}}{OD_{sample} - OD_{blank}} - \frac{F_{background} - F_{blank}}{OD_{background} - OD_{blank}} \qquad (1)$$

Here, *F* is the raw fluorescence of the given sample and *OD* is the OD of the given sample at 600 nm. Raw OD measurements for all experiments are provided in **Supplementary Figure 3-S7**. As expected, bacterial growth is highest in the physiological range of 35 ºC to 39 ºC. The value of blank fluorescence was determined as the average of all 96 wells in a qPCR plate filled with 25 µL LB. Blank OD was taken as the y-intercept of a standard curve of 90 µL non-fluorescent E. coli cultures whose OD_{600} values were determined by cuvette measurements in a Nanodrop 2000c spectrophotometer (96 samples total). Background fluorescence was measured from a non-fluorescent construct derived by mutating the chromophore of mWasabi [58] in the pTlpA-Wasabi plasmid (pTlpA-Wasabi-NF). Fluorescence measurements for the thermal expression landscapes of TlpA and TcI were performed using the plate reader due to signal saturation of the qPCR at the 24 hour time

point (Sample N = 3; Background N = 2 for each time point and temperature). Errors from background measurements were propagated by addition in quadrature. Errors from blank measurements were negligible relative to sample-to-sample variation (relative standard deviation < 2%) and were omitted from the calculation.

Colony Screening for TlpA Tuning

Error-prone PCR was performed on pTlpA-Wasabi (Stratagene GeneMorph II kit) and on pTcI-Wasabi (NEB Taq Polymerase/0.2 mM $MnCl_2$) and the PCR products were inserted into the parent constructs using Gibson Assembly. The resulting libraries were transformed into NEB10β *E. coli* and plated on LB Agar. Following overnight incubation at 30 °C and the appearance of colonies, a Replica-Plating Tool (VWR 25395-380) was used to replicate each seed plate into two receiver plates. One receiver plate was grown overnight at the desired repressed temperature, and the other at the intended activation temperature. Upon the appearance of visible colonies, plates were imaged in a Bio-Rad ChemiDoc MP imager using blue epifluorescent illumination and the 530/28 nm emission filter. Images were examined manually for colonies that appeared dark or invisible on the "off plate" but showed bright fluorescence on the "on plate". Approximately 10^3 colonies were screened per library. These colonies were picked and subjected to the liquid culture thermal activation assay described above, whereupon their thermal induction profile was compared to that of their parent plasmid. Variants that demonstrated sharp switching and large dynamic range between the desired new transition temperatures were sequenced, re-transformed, and assayed using a higher number of replicates.

In Vitro *Toxin-Antitoxin Assays*

NEB10β cells were transformed with the thermally regulated toxin-antitoxin plasmid and allowed to grow at 37 °C overnight. Because reversion of plasmids carrying toxic genes such as CcdB is known to be a common phenomenon, we used a replica plate screen to isolate colonies that maintained a functional thermal kill switch after transformation. To this end, we replica plated the original transformation into two new plates, one incubated at 25°C and the other maintained at 37 °C. Colonies that grew at the permissive temperature of 37 °C and not at 25°C were used in downstream *in vitro* or *in vivo* experiments. For *in vitro* experiments, the selected colonies were grown in 2xYT media with 100 µg/mL ampicillin at 37°C with shaking until OD_{600} of 0.6 whereupon they were diluted and plated onto LB agar plates. The plates were incubated overnight at either 25°C or 37°C, after which colony forming units (CFU) were counted.

Focused Ultrasound

MRI-guided focused ultrasound treatment was performed using a 16-channel ultrasound generator, motorized MRI-compatible transducer positioning system and an annular array transducer operating at 1.5 MHz (Image Guided Therapy, Pessac, France). Targeting and real-time imaging was performed using a Bruker Biospec/Avance 7T MRI system with RF excitation delivered by a 7.2 cm diameter volume coil and detection via a 3 cm diameter surface coil. Temperature monitoring was performed using a continuously applied Fast Low Angle Shot sequence with a T_R of 75 ms and T_E of 2.5 ms, matrix size of 32 x 32, and varying FOVs as listed below. Phase images were processed in real time using ThermoGuide software (Image Guided Therapy) and temperature was calculated from the per-pixel phase accumulation due to a decrease in proton precession frequency of 0.01 ppm/°C.

For *in vitro* heating, 100 μL of a saturated NEB10β culture expressing the temperature-inducible reporter circuit was plated overnight at 30 °C and incubated for approximately 12 hours to form a lawn on a plate containing 0.24 %w/v LB (Sigma) and 0.32 %w/v Bacto Agar (BD). An approximately 3 cm x 3 cm square of agar was excised from the plate and placed, with the bacterial side facing up, onto a comparably sized pad of 1 cm thick extra firm tofu (O Organics) coated with SCAN ultrasound gel (Parker Laboratories) to exclude air at the interface. A 1 cm high plastic washer made by drilling through the lid of a VWR 35 mm plastic tissue culture dish was placed onto the bacteria and the assembly was inverted and placed onto the surface coil such that the bacterial lawn, facing down, was supported by the washer. The ultrasound transducer was positioned above the assembly, in contact with the tofu through another thin layer of ultrasound gel. To provide a reference to compensate for global phase drift during the experiment, a second piece of tofu was placed within the field of view but spatially separated by a 1 cm air gap from the object under insonation. A fiber optic thermometer (Neoptix T1) was inserted into the reference tofu, and the difference between the MRI-derived reference temperature and thermometer-reported temperature was accounted for at the site of insonation when calculating the true focal heating.

Ultrasound was applied with the focus aimed at the tofu immediately adjacent to the agar layer with manual control of power level and duty cycle so as to maintain a temperature of 41.5–43 °C for 45 minutes. Imaging was performed as described above with a matrix size of 5.39 x 5.05 cm and a slice thickness of 2 mm. The plate was subsequently returned to 30 °C for 5 hours and imaged using a Bio-Rad ChemiDoc MP imager with blue epi illumination and a 530/28 nm emission filter (mWasabi) and also green epi illumination and a 605/50 nm filter (mCherry).

Animal Procedures

All animal procedures were performed under a protocol approved by the California Institute of Technology Institutional Animal Care and Use Committee (IACUC). 9-week old BALB/c female mice and 4-week old NU/J 2019 female mice were purchased from Jackson Laboratory (JAX); 4-week old SCID/SHC female mice were purchased from Charles River. For *in vivo* ultrasound actuation, *E. coli* expressing the pTlpA36-Wasabi plasmid were grown to OD 0.6, pelleted, and resuspended to OD 24. A 100 μL bolus was injected subcutaneously into both hindlimbs of a nude mouse (SCID or NU/J2019). Mice were anaesthetized using a 2% isoflurane-air mixture and placed on a dedicated animal bed with the surface coil positioned below the target limb of the mouse. Anesthesia was maintained over the course of the ultrasound procedure using 1–1.5% isoflurane. Respiration rate was maintained at 20–30 breaths per minute and temperature and respiration rate were continuously monitored using a pressure pad (Biopac Systems) and a fiber optic rectal thermometer (Neoptix). The target limb was thermally activated by elevating the temperature to 41°C and maintaining the elevated temperature for 45 min to 1 hour. Temperature monitoring and adjustment was performed as described above for *in vitro* experiments. Following ultrasound treatment, the mouse was returned to its cage for four hours, anaesthetized, and imaged using a Bio-Rad ChemiDoc MP imager with blue epi illumination and the 530/28 nm emission filter (mWasabi).

For host fever sensing experiments, SCID mice injected with bacteria as described above were housed in an incubator preset to 41°C for two hours and control mice were housed at room temperature. Following treatment, all mice were housed at room temperature for four

hours, anaesthetized, and imaged using a Bio-Rad ChemiDoc MP imager with blue epi illumination and the 530/28 nm emission filter (mWasabi).

Mouse images are representative of three independent *in vivo* experiments. Fever-induced and control mice were littermates randomly selected for each experimental condition. Investigators were not blinded to group allocation because no subjective evaluations were performed.

For host confinement experiments, BALB/c mice were given drinking water containing 0.5 mg/mL of ampicillin for 24h, and then starved for food overnight. *E.coli* were grown in 2xYT media containing ampicillin at 37°C with shaking until OD_{600} of 0.6. Cultures were pelleted and resuspended at 10^8 cells/mL in PBS containing 1.5% $NaHCO_3$. 200 µL of the suspension was administered orally using a gavage needle. Food was returned to the mice and the drinking water contained ampicillin throughout the entire experiment. Fresh fecal samples were collected from each mouse 5 hrs after gavage and incubated at 37°C or 25°C for 24h, then weighed, homogenized in PBS at 0.1 g/mL, diluted and plated onto LB agar plates containing ampicillin. Plates were then incubated overnight at 25°C and 37°C. Bacterial colonies were counted as described above for *in vitro* toxin-antitoxin experiments. The sample size was N = 5 mice, which was chosen based on preliminary experiments indicating that it would be sufficient to detect significant differences in mean values.

Electrophoretic Mobility Shift Assay

Interaction between TlpA, σ^{70}-RNAp holoenzyme and DNA was demonstrated using a gel shift assay. For this, 50 pmoles of fluorescein-labeled double stranded DNA representing the TlpA operator with flanking padding sequences (70 base pairs in total) was incubated with either 50 pmoles of TlpA protein or 5 Units (8.5 pmoles) σ^{70}-RNAp holoenzyme (NEB

M0551S) individually in 50 uL reaction buffer comprising 40 mM Tris-HCl, 150 mM KCl, 10mM MgCl2, .01% Triton-X-100 and 1 mM DTT at a pH of 7.5. As a negative control, the wildtype TlpA operator was replaced with a scrambled version. Following incubation at 37ºC for 30 minutes, 10 uL of the reaction mixture was supplemented with glycerol to a final concentration of 5 % and loaded in a nondenaturing 4 % polyacrylamide resolving gel. The gel was run at 65 V for 90 minutes in buffer comprising 45 mM Tris-borate and 1 mM EDTA at a pH of 8.3. DNA was visualized using Bio-Rad ChemiDoc MP imager using blue epifluorescent illumination and the 530/28 nm emission filter.

Statistics and Replicates

Data is plotted and reported in the text as the mean ± SEM. Sample size is N = 4 biological replicates in all *in vitro* experiments unless otherwise stated. This sample size was chosen based on preliminary experiments indicating that it would be sufficient to detect significant differences in mean values. P-values were calculated using a two-tailed unpaired heteroscedastic t-test.

3.5: References

1. Ford, T.J. & Silver, P.A. Synthetic biology expands chemical control of microorganisms. *Current opinion in chemical biology* **28**, 20-28 (2015).
2. Fischbach, M.A., Bluestone, J.A. & Lim, W.A. Cell-based therapeutics: the next pillar of medicine. *Science translational medicine* **5**, 179ps177-179ps177 (2013).
3. Steidler, L. et al. Treatment of murine colitis by Lactococcus lactis secreting interleukin-10. *Science* **289**, 1352-1355 (2000).
4. Daniel, C., Roussel, Y., Kleerebezem, M. & Pot, B. Recombinant lactic acid bacteria as mucosal biotherapeutic agents. *Trends in biotechnology* **29**, 499-508 (2011).
5. Claesen, J. & Fischbach, M.A. Synthetic microbes as drug delivery systems. *ACS synthetic biology* **4**, 358-364 (2014).
6. Wells, J.M. & Mercenier, A. Mucosal delivery of therapeutic and prophylactic molecules using lactic acid bacteria. *Nature Reviews Microbiology* **6**, 349-362 (2008).
7. Courbet, A., Endy, D., Renard, E., Molina, F. & Bonnet, J. Detection of pathological biomarkers in human clinical samples via amplifying genetic switches and logic gates. *Science translational medicine* **7**, 289ra283-289ra283 (2015).
8. Danino, T. et al. Programmable probiotics for detection of cancer in urine. *Science translational medicine* **7**, 289ra284-289ra284 (2015).
9. Kotula, J.W. et al. Programmable bacteria detect and record an environmental signal in the mammalian gut. *Proceedings of the National Academy of Sciences* **111**, 4838-4843 (2014).
10. Archer, E.J., Robinson, A.B. & Süel, G.r.M. Engineered E. coli that detect and respond to gut inflammation through nitric oxide sensing. *ACS synthetic biology* **1**, 451-457 (2012).
11. Ntziachristos, V. Going deeper than microscopy: the optical imaging frontier in biology. *Nature methods* **7**, 603-614 (2010).
12. Haar, G.T. & Coussios, C. High intensity focused ultrasound: physical principles and devices. *International journal of hyperthermia : the official journal of European Society for Hyperthermic Oncology, North American Hyperthermia Group* **23**, 89-104 (2007).
13. Huang, X., El-Sayed, I.H., Qian, W. & El-Sayed, M.A. Cancer cell imaging and photothermal therapy in the near-infrared region by using gold nanorods. *Journal of the American Chemical Society* **128**, 2115-2120 (2006).
14. Thiesen, B. & Jordan, A. Clinical applications of magnetic nanoparticles for hyperthermia. *International journal of hyperthermia* **24**, 467-474 (2008).
15. Zhao, K., Liu, M. & Burgess, R.R. The global transcriptional response of Escherichia coli to induced sigma 32 protein involves sigma 32 regulon activation followed by inactivation and degradation of sigma 32 in vivo. *The Journal of biological chemistry* **280**, 17758-17768 (2005).
16. de Marco, A., Vigh, L., Diamant, S. & Goloubinoff, P. Native folding of aggregation-prone recombinant proteins in Escherichia coli by osmolytes, plasmid- or benzyl alcohol-overexpressed molecular chaperones. *Cell stress & chaperones* **10**, 329-339 (2005).
17. Inda, M.E. et al. A lipid-mediated conformational switch modulates the thermosensing activity of DesK. *Proceedings of the National Academy of Sciences* **111**, 3579-3584 (2014).
18. Kortmann, J., Sczodrok, S., Rinnenthal, J., Schwalbe, H. & Narberhaus, F. Translation on demand by a simple RNA-based thermosensor. *Nucleic Acids Res* **39**, 2855-2868 (2011).
19. Neupert, J., Karcher, D. & Bock, R. Design of simple synthetic RNA thermometers for temperature-controlled gene expression in Escherichia coli. *Nucleic Acids Res* **36**, e124 (2008).
20. Waldminghaus, T., Kortmann, J., Gesing, S. & Narberhaus, F. Generation of synthetic RNA-based thermosensors. *Biological chemistry* **389**, 1319-1326 (2008).

21. Hoynes-O'Connor, A., Hinman, K., Kirchner, L. & Moon, T.S. De novo design of heat-repressible RNA thermosensors in E. coli. *Nucleic acids research* **43**, 6166-6179 (2015).
22. Satija, R., Sen, S., Siegal-Gaskins, D. & Murray, R.M. Design of a Toolbox of RNA Thermometers. *bioRxiv*, 017269 (2015).
23. Waldminghaus, T., Kortmann, J., Gesing, S. & Narberhaus, F. Generation of synthetic RNA-based thermosensors. *Biological chemistry* **389**, 1319-1326 (2008).
24. Neupert, J., Karcher, D. & Bock, R. Design of simple synthetic RNA thermometers for temperature-controlled gene expression in Escherichia coli. *Nucleic acids research* **36**, e124-e124 (2008).
25. Wieland, M. & Hartig, J.S. RNA quadruplex-based modulation of gene expression. *Chemistry & biology* **14**, 757-763 (2007).
26. Hurme, R., Berndt, K.D., Namork, E. & Rhen, M. DNA binding exerted by a bacterial gene regulator with an extensive coiled-coil domain. *The Journal of biological chemistry* **271**, 12626-12631 (1996).
27. Valdez-Cruz, N.A., Caspeta, L., Perez, N.O., Ramirez, O.T. & Trujillo-Roldan, M.A. Production of recombinant proteins in E. coli by the heat inducible expression system based on the phage lambda pL and/or pR promoters. *Microbial cell factories* **9**, 18 (2010).
28. Sussman, R. & Jacob, F. Sur un systeme de repression thermosensible chez le bacteriophage lambda d'Escherichia coli. *Comptes rendus hebdomadaires des séances de l'Académie des sciences*, 1517-1519 (1962).
29. Wissmann, A. et al. Selection for Tn10 tet repressor binding to tet operator in Escherichia coli: isolation of temperature-sensitive mutants and combinatorial mutagenesis in the DNA binding motif. *Genetics* **128**, 225-232 (1991).
30. Chao, Y.P., Chern, J.T., Wen, C.S. & Fu, H. Construction and characterization of thermo-inducible vectors derived from heat-sensitive lacI genes in combination with the T7 A1 promoter. *Biotechnology and bioengineering* **79**, 1-8 (2002).
31. McCabe, K.M., Lacherndo, E.J., Albino-Flores, I., Sheehan, E. & Hernandez, M. LacI(Ts)-regulated expression as an in situ intracellular biomolecular thermometer. *Applied and environmental microbiology* **77**, 2863-2868 (2011).
32. Hurme, R., Berndt, K.D., Normark, S.J. & Rhen, M. A proteinaceous gene regulatory thermometer in Salmonella. *Cell* **90**, 55-64 (1997).
33. Wilson, C.J., Zhan, H., Swint-Kruse, L. & Matthews, K.S. The lactose repressor system: paradigms for regulation, allosteric behavior and protein folding. *Cellular and molecular life sciences : CMLS* **64**, 3-16 (2007).
34. Bertram, R. & Hillen, W. The application of Tet repressor in prokaryotic gene regulation and expression. *Microbial biotechnology* **1**, 2-16 (2008).
35. Jensen, P.R., Westerhoff, H.V. & Michelsen, O. The use of lac-type promoters in control analysis. *European journal of biochemistry / FEBS* **211**, 181-191 (1993).
36. Altschul, S.F. et al. Gapped BLAST and PSI-BLAST: a new generation of protein database search programs. *Nucleic acids research* **25**, 3389-3402 (1997).
37. Al-Bataineh, O., Jenne, J. & Huber, P. Clinical and future applications of high intensity focused ultrasound in cancer. *Cancer treatment reviews* **38**, 346-353 (2012).
38. Elias, W.J. et al. A pilot study of focused ultrasound thalamotomy for essential tremor. *New England Journal of Medicine* **369**, 640-648 (2013).
39. Deckers, R. et al. Image-guided, noninvasive, spatiotemporal control of gene expression. *Proceedings of the National Academy of Sciences* **106**, 1175-1180 (2009).
40. Fite, B.Z. et al. Magnetic resonance thermometry at 7T for real-time monitoring and correction of ultrasound induced mild hyperthermia. *PloS one* **7**, e35509 (2012).

41. McDannold, N.J., King, R.L., Jolesz, F.A. & Hynynen, K.H. Usefulness of MR Imaging-Derived Thermometry and Dosimetry in Determining the Threshold for Tissue Damage Induced by Thermal Surgery in Rabbits 1. *Radiology* **216**, 517-523 (2000).
42. McDannold, N., Vykhodtseva, N., Jolesz, F.A. & Hynynen, K. MRI investigation of the threshold for thermally induced blood–brain barrier disruption and brain tissue damage in the rabbit brain. *Magnetic resonance in medicine* **51**, 913-923 (2004).
43. Rudaya, A.Y., Steiner, A.A., Robbins, J.R., Dragic, A.S. & Romanovsky, A.A. Thermoregulatory responses to lipopolysaccharide in the mouse: dependence on the dose and ambient temperature. *American journal of physiology. Regulatory, integrative and comparative physiology* **289**, R1244-1252 (2005).
44. Pritchard, M.T. et al. Protocols for simulating the thermal component of fever: preclinical and clinical experience. *Methods (San Diego, Calif.)* **32**, 54-62 (2004).
45. Illing, A.C., Shawki, A., Cunningham, C.L. & Mackenzie, B. Substrate profile and metal-ion selectivity of human divalent metal-ion transporter-1. *Journal of Biological Chemistry* **287**, 30485-30496 (2012).
46. Nistala, G.J., Wu, K., Rao, C.V. & Bhalerao, K.D. A modular positive feedback-based gene amplifier. *Journal of biological engineering* **4**, 4 (2010).
47. Andersen, J.B. et al. New unstable variants of green fluorescent protein for studies of transient gene expression in bacteria. *Applied and environmental microbiology* **64**, 2240-2246 (1998).
48. Natori, Y., Kano, Y. & Imamoto, F. Characterization and promoter selectivity of Lactobacillus acidophilus RNA polymerase. *Biochimie* **70**, 1765-1774 (1988).
49. Mimee, M., Tucker, A.C., Voigt, C.A. & Lu, T.K. Programming a human commensal bacterium, Bacteroides thetaiotaomicron, to sense and respond to stimuli in the murine gut microbiota. *Cell systems* **1**, 62-71 (2015).
50. Tey, S.-K. Adoptive T-cell therapy: adverse events and safety switches. *Clinical & translational immunology* **3**, e17 (2014).
51. Chan, C.T., Lee, J.W., Cameron, D.E., Bashor, C.J. & Collins, J.J. 'Deadman' and 'Passcode' microbial kill switches for bacterial containment. *Nat Chem Biol* **12**, 82-86 (2016).
52. Gallagher, R.R., Patel, J.R., Interiano, A.L., Rovner, A.J. & Isaacs, F.J. Multilayered genetic safeguards limit growth of microorganisms to defined environments. *Nucleic Acids Res* **43**, 1945-1954 (2015).
53. Lang, K. & Chin, J.W. Cellular incorporation of unnatural amino acids and bioorthogonal labeling of proteins. *Chemical reviews* **114**, 4764-4806 (2014).
54. Handley, A., Schauer, T., Ladurner, A.G. & Margulies, C.E. Designing cell-type-specific genome-wide experiments. *Molecular cell* **58**, 621-631 (2015).
55. Grammel, M. & Hang, H.C. Chemical reporters for biological discovery. *Nature chemical biology* **9**, 475-484 (2013).
56. Ai, H.W., Olenych, S.G., Wong, P., Davidson, M.W. & Campbell, R.E. Hue-shifted monomeric variants of Clavularia cyan fluorescent protein: identification of the molecular determinants of color and applications in fluorescence imaging. *BMC biology* **6**, 13 (2008).
57. Shaner, N.C. et al. Improved monomeric red, orange and yellow fluorescent proteins derived from Discosoma sp. red fluorescent protein. *Nature biotechnology* **22**, 1567-1572 (2004).
58. Wielgus-Kutrowska, B., Narczyk, M., Buszko, A., Bzowska, A. & Clark, P.L. Folding and unfolding of a non-fluorescent mutant of green fluorescent protein. *Journal of Physics: Condensed Matter* **19**, 285223 (2007).

3.6: Supplementary Results

Supplementary Table 3-T1 – Mutant and wild type bioswitch performance

Variant	Fold Change	SEM (±)	T_{off}	T_{max}
TlpA	355	45	31.4	44.6
$TlpA_{36}$	370	63	31.4	44.6
$TlpA_{39}$	1523	434	31.4	44.6
TcI	1432	404	34.2	40
TcI_{38}	1032	160	32.4	40
TcI_{42}	1692	444	32.4	45.7

***** The reported T_{off} for each variant is the lowest temperature at which fluorescence could be detected above noise. T_{max} is the temperature at which fluorescence was maximal.

Supplementary Table 3-T2 – Genetic constructs used in the study

All plasmids were constructed using the pETDuet-1 backbone (EMD Biosciences) with the relevant thermal biosensor elements replacing multiple cloning sites 1 and 2.

Plasmid	Transcriptional Regulator(s)	Output Gene Product(s)
pTlpA-Wasabi	TlpA	mWasabi
pTlpA-Wasabi-NF	TlpA	Nonfluorescent mWasabi (S71T, G73A)
pTcI-Wasabi	TcI (cI852 Repressor, cI A67T)	mWasabi
pLacI241-Wasabi	LacI A241T (mutation made in pETDuet-1 LacI)	mWasabi
pLacI265-Wasabi	LacI G265D (mutation made in pETDuet-1 LacI)	mWasabi
pTetR89-Wasabi	TetR A89D	mWasabi
pTetR193-Wasabi	TetR I193N	mWasabi
pLon-Wasasbi	Lon Promoter (GenBank CP009072)	mWasabi
pRpoH-Wasabi	RpoH Promoter (GenBank CP009072)	mWasabi
pClp-Wasabi	ClpP-ClpX Promoter (Genbank CP009072)	mWasabi
pHtpG-Wasabi	HtpG Promoter (Genbank CP009072)	mWasabi
pDnaK-Wasabi	DnaK Promoter (Genbank CP009072)	mWasabi
pGrpE-Wasabi	GrpE Promoter (Genbank CP009072)	mWasabi
pLacIq-Wasabi	LacIq Promoter	mWasabi
$pTlpA_{SP}$-Wasabi	TlpA Promoter with putative Pribnow box scrambled	mWasabi
$pTlpA_{Reverse}$-Wasabi	TlpA Promoter as reverse complement	mWasabi
$pTlpA_{36}$-Wasabi	$TlpA_{36}$	mWasabi
$pTlpA_{39}$-Wasabi	$TlpA_{39}$	mWasabi
$pTcI_{38}$-Wasabi	TcI_{38}	mWasabi
$pTcI_{42}$-Wasabi	TcI_{42}	mWasabi
pCali2	$TlpA_{36}$, TcI	mWasabi, mCherry
pThermeleon	TcI, TlpA, cI_{wt} (under control of TlpA)	mWasabi, mCherry
pKillswitch	$TlpA_{36}$	CcdA with SsrA degradation tag

Sources of genetic elements: TlpA: B. Finlay, Univ. British Columbia; mWasabi: F. Arnold, Caltech; mCherry: S. Qi, Stanford; CcdB: pLenti X1 Zeo DEST plasmid (Addgene #17299); TetR: pENTR1A plasmid (Addgene #22265); all other elements: Gblock synthesis (IDT).

Supplementary Table 3-T3 – List of mutations in selected variants of TlpA and TcI

Construct	Nonsynonymous Mutations	Synonymous Mutations
$TlpA_{36}$	P60L, D135V, K187R, K202I, L208Q	
$TlpA_{39}$	D135V, A217V, L236F	
TcI_{38}	M1V, L65S, K68R, F115L, D126G, D188G	A50 (GCT -> GCC), E128 (GAG -> GAA), R129 (AGA -> AGG), T152 (ACA -> ACC), L185 (CTT -> CTC)
TcI_{42}	K6N, S33T, Y61H, L119P, F122C	L51 (TTA -> CTA)

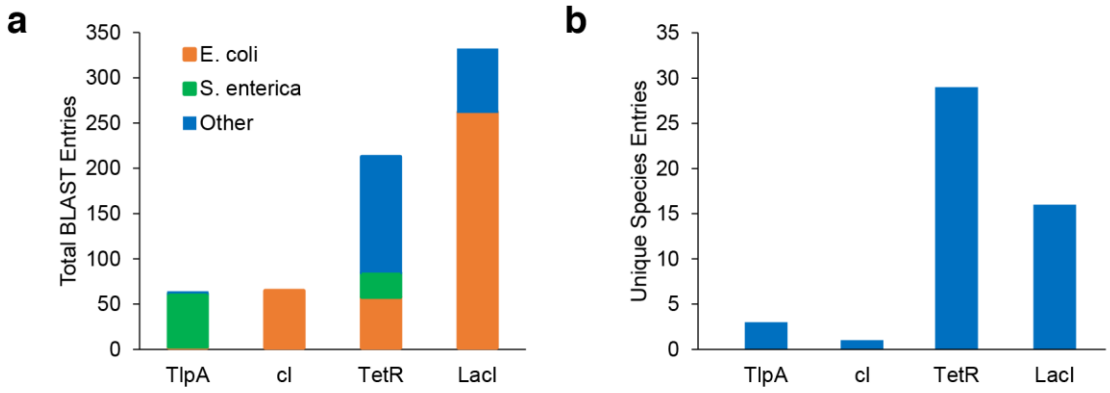

Supplementary Figure 3-S1 – Prevalence of repressor sequences in bacteria. (**a**) National Center for Biotechnology Information (NCBI) Basic Local Alignment Search Tool (BLAST) search results for the wild type tlpA, cI, tetR, and lacI genes showing the cumulative number of hits obtained. The NCBI nucleotide collection was searched with the source organism restricted to bacteria. Cloning vectors, synthetic constructs, and individual gene sequences were omitted; genomic and naturally occurring plasmid sequences were retained. Sequences with alignment lengths of less than 90% of the wild type protein sequence were not included. The lacI gene is distributed throughout many commonly utilized *E. coli* strains such as Nissle 1917 and BL21, whereas the cI gene is found in less widely used *E. coli* strains. (**b**) The number of bacterial species in which the selected repressors are found. Data were obtained as in (**a**) and substrains were binned together. TlpA is largely restricted to *S. enterica* and cI to *E. coli*; tetR and lacI can be found in a larger number of bacterial species.

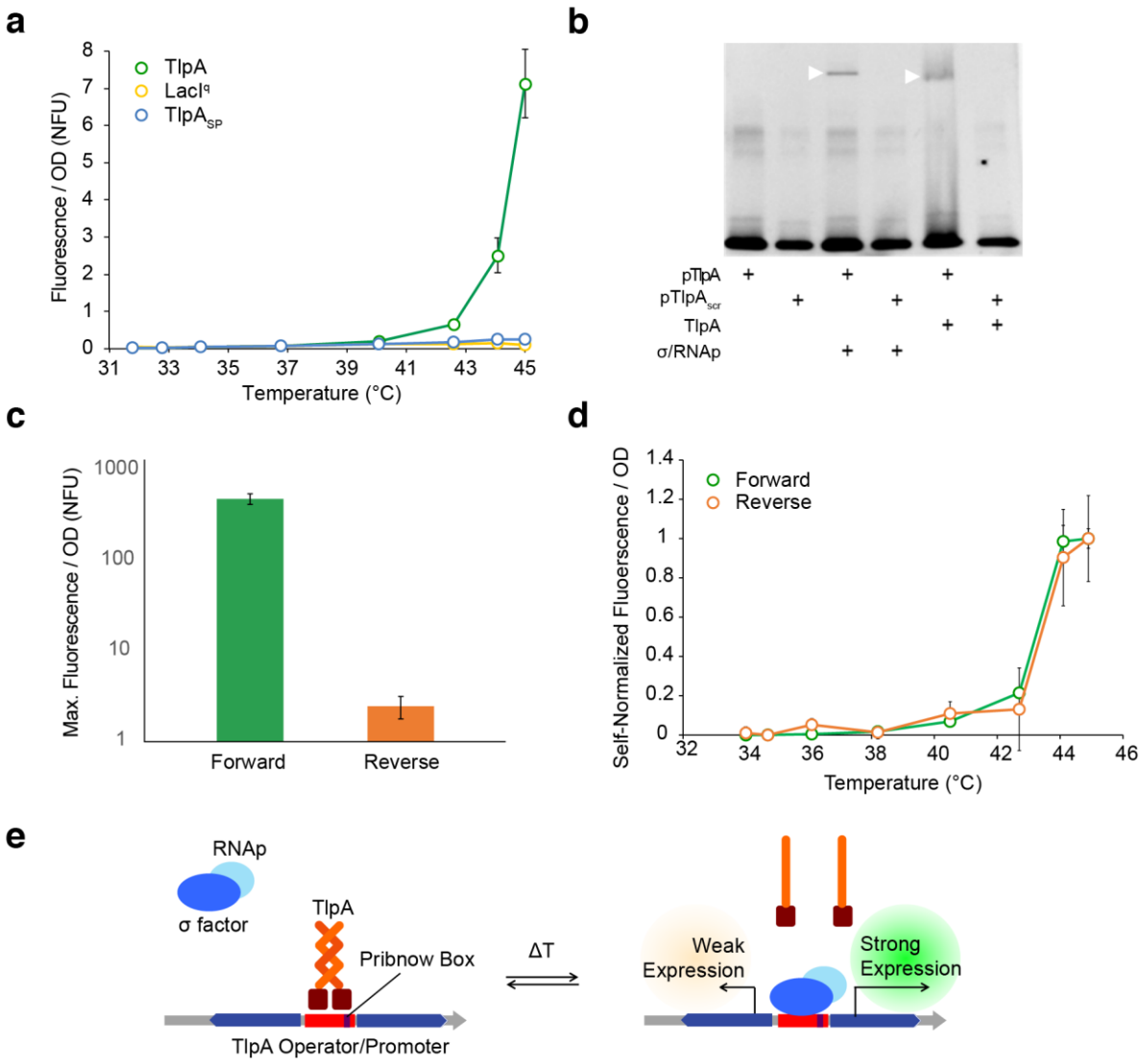

Supplementary Figure 3-S2 – Mechanisms and bidirectional activity of the TlpA operator. (**a**) OD-normalized expression of the GFP reporter gene under the control of TlpA, $LacI^q$, and $TlpA_{SP}$ (in which nucleotides within the Pribnow box of the operator are shuffled). (**b**) Electromobility shift assay using a FAM-labeled TlpA operator oligonucleotide, demonstrating association of the operator with both TlpA and the *E. coli* σ^{70}-RNAp holoenzyme. In contrast, scrambled TlpA operator fails to associate with these proteins. The TlpA and σ^{70}-RNAp concentrations used in this experiment (1 µM and 0.18 µM, respectively) were similar to previous literature.[7,8] (**c**) GFP expression driven by the TlpA operator in the canonical and flipped orientations at 44.1ºC. (**d**) Thermal induction profiles for GFP expression under the control of forward and reverse-oriented TlpA operator. Each curve is self-normalized to its maximal fluorescence intensity. (**e**) Proposed mechanism of TlpA-based thermal transcriptional regulation.

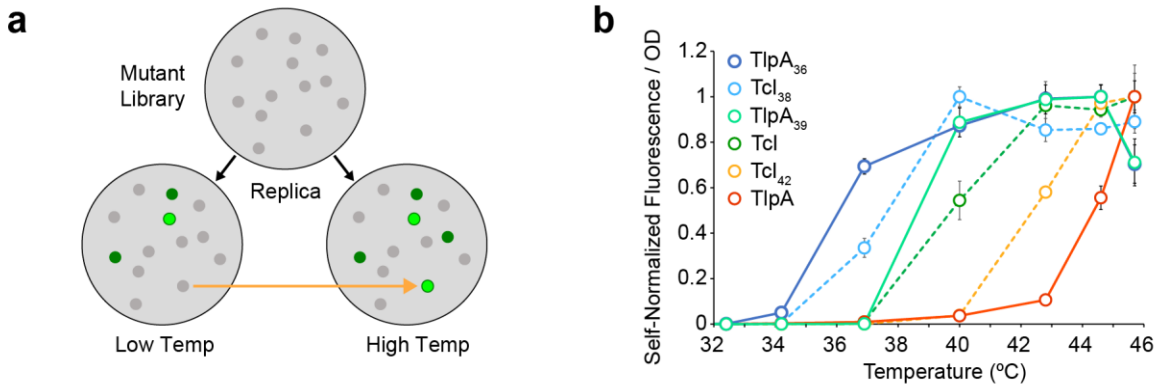

Supplementary Figure 3-S3 - Tuning the transition temperature of thermal bioswitches. (**a**) Illustration of the screening strategy used to identify temperature-shifted repressor variants. (**b**) Self-normalized fluorescence/OD profiles for the full set of TlpA (solid lines) and TcI (dashed lines) bioswitches, demonstrating the complete range of available transition temperatures.

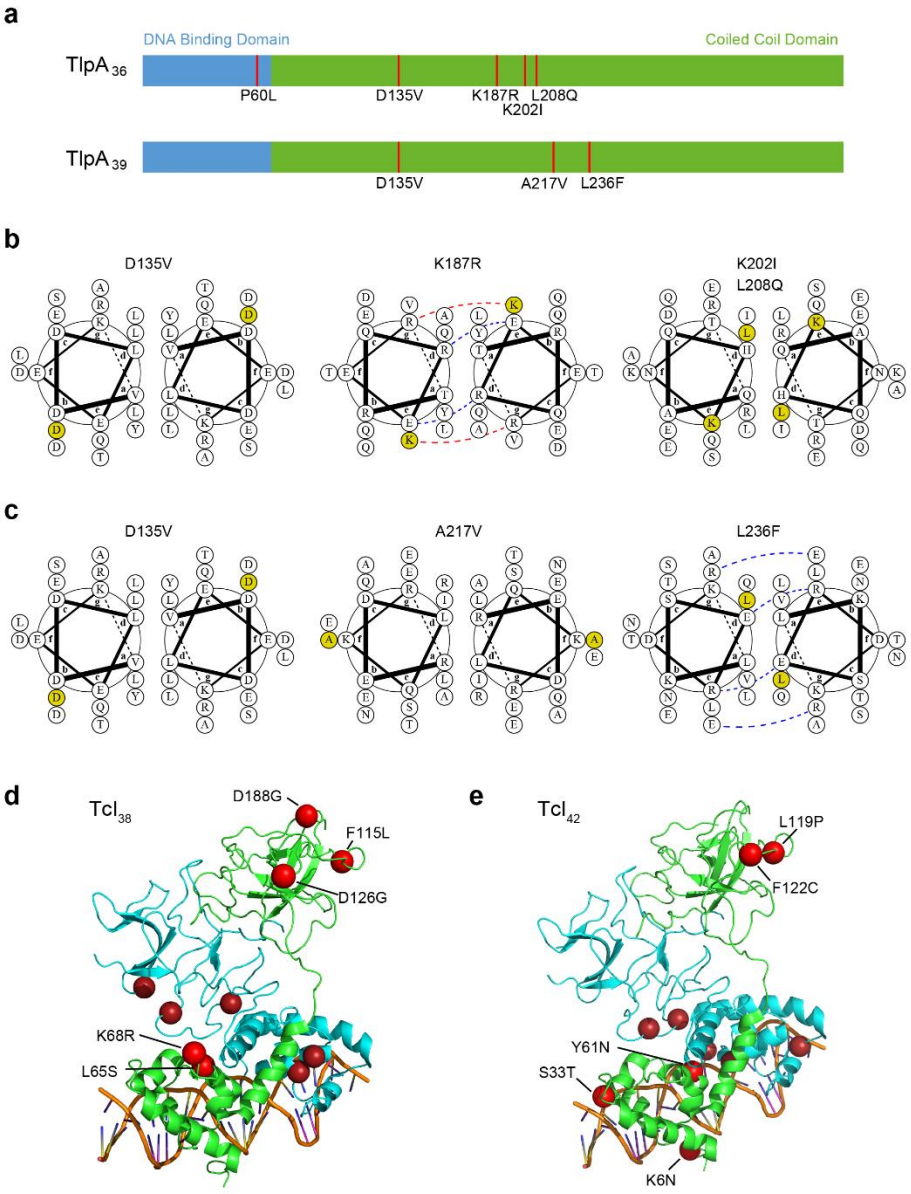

Supplementary Figure 3-S4 – Positions of mutations in selected variants of TlpA and TcI. (**a**) Schematic of mutation positions (red) within the predicted domain structure of $TlpA_{36}$ and $TlpA_{39}$. The DNA binding domain is depicted in blue and coiled-coil domain in green, as delineated by Koski et al[1]. The figure is drawn to the scale of the primary sequence. (**b**) Positions of mutations in $TlpA_{36}$ within the predicted structure of the coiled-coil interface as viewed down the long axis of the helix. Blue dashed lines represent predicted energetically favorable ionic interactions; red dashes indicate predicted repulsive ionic interactions. The coil register was assigned based on consensus between previous literature[1] and the structure prediction servers COILS[2], Paircoil2[3], and LOGICOIL[4]. The images were produced using DrawCoil 1.0[5]. The P60L mutation is not shown because it falls outside of the predicted coiled-coil region. (**c**) Positions of mutations in $TlpA_{39}$. Register prediction and illustration were performed as in (b). (**d**) Mutation positions (red) for the lambda repressor variant TcI_{38}. The crystal structure of the wild type lambda repressor (PDB code 3BDN) was used as the homology model[6]. The original temperature-sensitizing mutation A67T is not shown. The M1V

mutation is not depicted because residue 1 was not reported in the crystal structure. (**e**) Mutation positions (red) within the TcI_{42} variant.

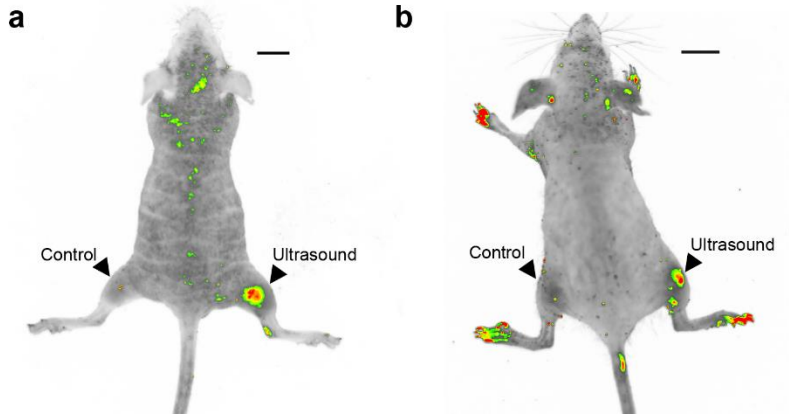

Supplementary Figure 3-S5 – Additional mice with ultrasound-activated gene expression. (**a**) and (**b**) Additional mice that underwent the experiment shown in Fig. 4e. The images are thresholded fluorescence maps of mice injected subcutaneously in both left and right hindlimbs with *E. coli* expressing GFP under the control of $TlpA_{36}$, following ultrasound activation at only the right hindlimb. Signal at mouse digits is the result of autofluorescence and varies from mouse to mouse; digits were neither injected with bacteria nor exposed to ultrasound.

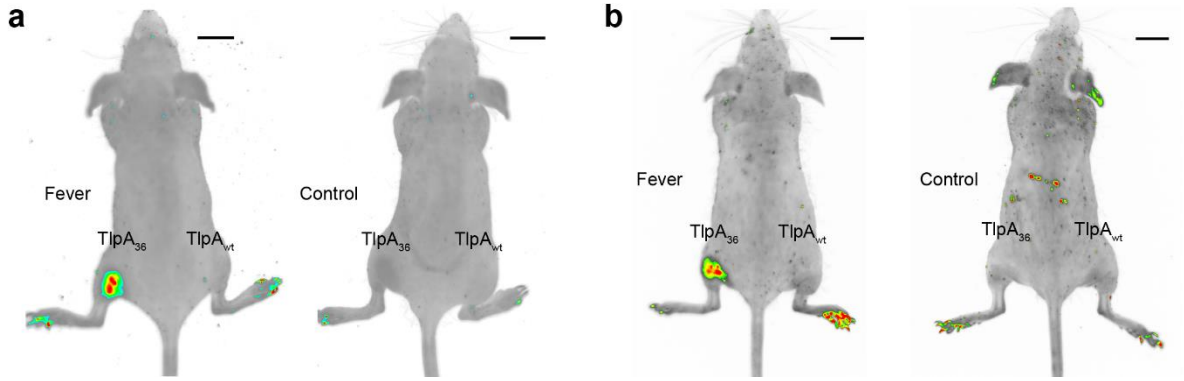

Supplementary Figure 3-S6 – Additional mice with fever-activated gene expression. (**a**) and (**b**) Additional pairs of mice that underwent the experiment shown in Fig. 5, b-c. Each panel shows thresholded fluorescence maps of one mouse that underwent fever induction after being injected subcutaneously with plasmids expressing $TlpA_{36}$- and TlpA-regulated GFP into the left and right hind limbs, respectively, with a paired mouse that was prepared identically but maintained at room temperature.

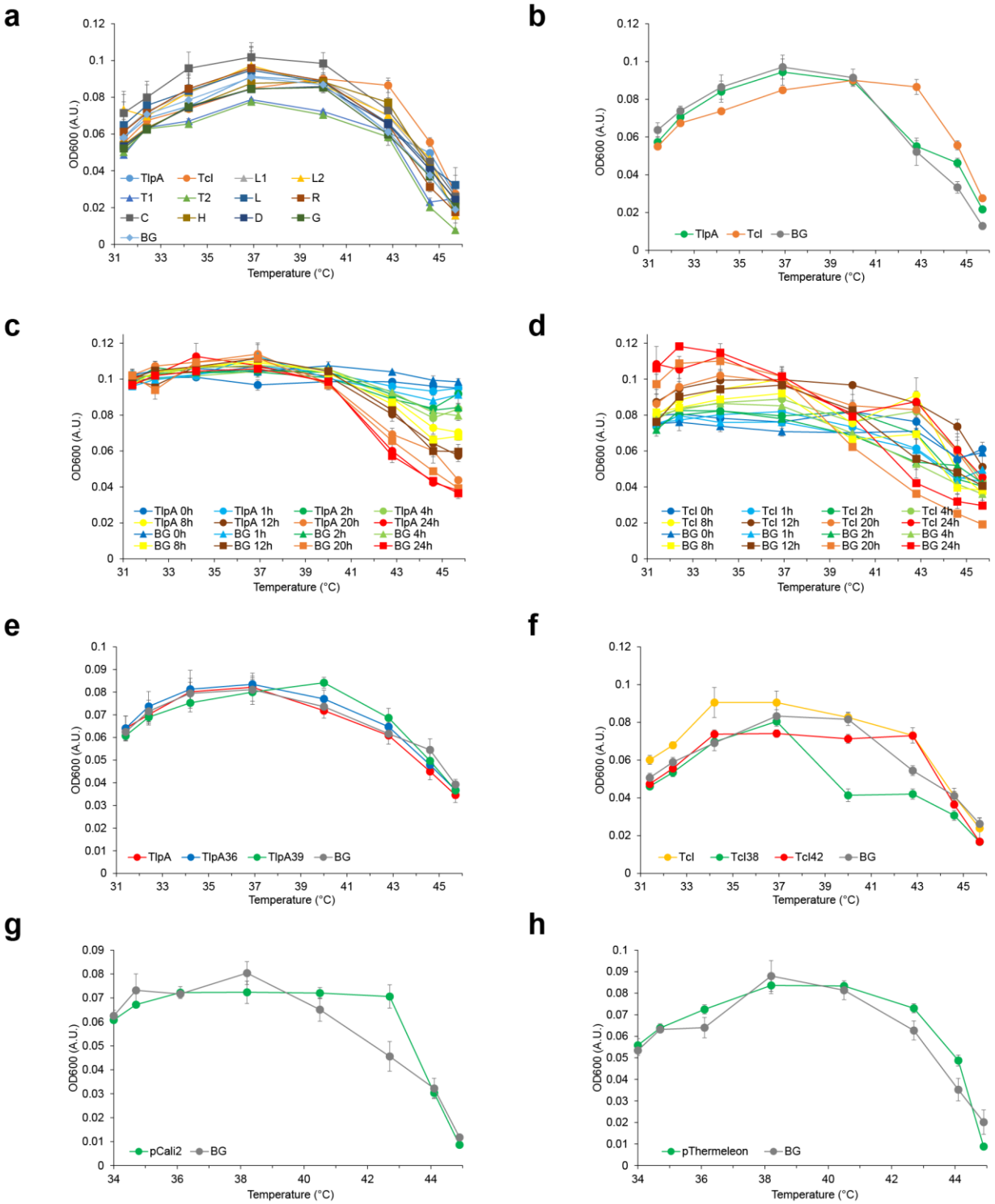

Supplementary Figure 3-S7. OD_{600} measurements for thermal induction profiles reported in main text. Blank-subtracted measurements of OD_{600} in 90 µL volumes in clear-bottom 96 well plates, corresponding to an optical path length of approximately 1.4 mm. Data corresponds to: (**a**) Fig. 1b; (**b**) Fig. 1c; (**c**) Fig. 1e; (**d**) Fig. 1f; (**e**) Fig. 2d; (**f**) Fig. 2e; (**g**) Fig. 3c; (**h**) Fig. 3g. BG = background.

3.7: Supplementary References

1. Koski, P., Saarilahti, H., Sukupolvi, S., Taira, S., Riikonen, P., Osterlund, K., … Rhen, M. A new alpha-helical coiled coil protein encoded by the Salmonella typhimurium virulence plasmid. *The Journal of Biological Chemistry* **267**, 12258–12265 (1992).
2. Lupas, A., Van Dyke, M., and Stock, J. Predicting Coiled Coils from Protein Sequences. *Science* **252**, 1162-1164 (1991).
3. McDonnel, A.V., Jiang, T., Keating, A.E., Berger B. Paircoil2: Improved prediction of coiled coils from sequence. *Bioinformatics* **22**, 356-358 (2006).
4. Vincent, T.L., Green, P.J., Woolfson, D.N. LOGICOIL—multi-state prediction of coiled-coil oligomeric state. *Bioinformatics* **29**, 69-76 (2013).
5. Grigoryan, G., Keating, A.E. Structural Specificity in Coiled-coil Interactions. *Current Opinion in Structural Biology* **18**, 477-483 (2008).
6. Stayrook. S.E., Jaru-Ampornpan, P., Ni, J., Hochschild, A., Lewis, M. Crystal structure of the lambda repressor and a model for pairwise cooperative operator binding. *Nature* **452**, 1022-1025 (2008).
7. Hurme, R., Berndt, K. D., Namork, E. & Rhen, M. DNA binding exerted by a bacterial gene regulator with an extensive coiled-coil domain. *The Journal of biological chemistry* **271**, 12626-12631 (1996).
8. Marr, M. T. & Roberts, J. W. Promoter Recognition As Measured by Binding of Polymerase to Nontemplate Strand Oligonucleotide. *Science* **276**, 1258-1260 (1997).

3.8: Detailed Author Contributions

Figure 3-1: DP designed and performed experiments.

Figure 3-2: DP and MA jointly designed experiments.

- MA performed experiment for **Fig. 3-2a**.
- MA collected data and DP performed analysis on **Fig. 3-2b**.
- MA performed experiment for **Fig. 3-2c**.
- DP performed experiment for **Fig. 3-2d**.

Figure 3-3: DP designed and performed experiments.

Figure 3-4:

- DP designed and performed experiments for **Fig 3-4 a-c**.
- MA designed and performed experiments for **Fig 3-4 d,e**.

Figure 3-5:

- MA designed and performed experiments for **Fig. 3-5 a-c**.
- MA designed experiment; MA and ALG collected data for **Fig. 3-5 d-f**.

Supplementary Figures

- **Fig 3-S1**: DP performed analysis.
- **Fig 3-S2**: DP designed and performed experiments for **S3-2 a, c, and d**. MA designed and performed experiments for **S3-2b**.
- **Fig. 3-S4**: DP performed analysis.
- **Fig. 3-S5**: MA and DP jointly performed experiment.
- **Fig. 3-S6**: MA performed experiment.